

Article

TiO₂-Photocatalyzed Water Depollution, a Strong, yet Selective Depollution Method: New Evidence from the Solar Light Induced Degradation of Glucocorticoids in Freshwaters

Luca Pretali, Angelo Albini , Alice Cantalupi, Federica Maraschi , Stefania Nicolis  and Michela Sturini * 

Department of Chemistry, University of Pavia, via Taramelli 12, 27100 Pavia, Italy; luca.pretali@gmail.com (L.P.); angelo.albini@unipv.it (A.A.); alice.cantalupi01@universitadipavia.it (A.C.); federica.maraschi@unipv.it (F.M.); stefania.nicolis@unipv.it (S.N.)

* Correspondence: michela.sturini@unipv.it; Tel.: +39-0382-987347

Abstract: The photodegradation of the most prescribed glucocorticoids (GCs) was studied under relevant environmental conditions in the presence of suspended TiO₂. The considered drugs included cortisone (CORT), hydrocortisone (HCORT), betamethasone (BETA), dexamethasone (DEXA), prednisone (PRED), prednisolone (PREDLO), and triamcinolone (TRIAM). The experiments were carried out at concentrations (50 µg L⁻¹) close to the real ones in freshwater samples (tap and river) under simulated and natural sunlight, and their decomposition took place very efficiently under natural sunlight. The reactions were monitored by high-pressure liquid chromatography coupled to electrospray ionization tandem mass spectrometry (HPLC-ESI-MS/MS). According to a pseudo-first-order decay, all drugs underwent degradation within 15 min, following different paths with respect to the direct photolysis. The observed kinetic constants, slightly lower in river than in tap water, varied from 0.29 to 0.61 min⁻¹ with modest differences among GCs in the same matrix. Among main matrix macro-constituents, humic acids (HAs) were the most interfering species involved in GCs degradation. The photogenerated primary products were identified by HPLC-ESI-MS/MS, allowing to elucidate the general photochemical path of GCs. Finally, a comparison with literature data obtained using different advanced oxidation processes (AOPs) highlights the treatment efficiency with TiO₂/solar light for removing such persistent aquatic contaminants.

Keywords: glucocorticoids; TiO₂-solar light degradation; freshwater pollution; photoproducts; matrix constituents



Citation: Pretali, L.; Albini, A.; Cantalupi, A.; Maraschi, F.; Nicolis, S.; Sturini, M. TiO₂-Photocatalyzed Water Depollution, a Strong, yet Selective Depollution Method: New Evidence from the Solar Light Induced Degradation of Glucocorticoids in Freshwaters. *Appl. Sci.* **2021**, *11*, 2486. <https://doi.org/10.3390/app11062486>

Academic Editor: Bin Gao

Received: 14 February 2021

Accepted: 6 March 2021

Published: 11 March 2021

Publisher's Note: MDPI stays neutral with regard to jurisdictional claims in published maps and institutional affiliations.



Copyright: © 2021 by the authors. Licensee MDPI, Basel, Switzerland. This article is an open access article distributed under the terms and conditions of the Creative Commons Attribution (CC BY) license (<https://creativecommons.org/licenses/by/4.0/>).

1. Introduction

The role of glucocorticoids in biochemistry is difficult to exaggerate. The many possible configurations and the various chemical functions present explain the variety of reactions they catalyze in the cell and the sophisticated machinery that, starting from the regulation of glucocorticoid secretion by the hypothalamic-pituitary-adrenal (HPA), governs virtually all of the physiological processes, such as metabolism, immune and cardiovascular functions, skeletal growth, reproduction, and cognition [1,2]. Specifically, glucocorticoids (GCs) can inhibit immunological, inflammatory, and allergic processes in our body in response to an outer stimulus. Since their coming in the 1950s, many synthetic molecules have been synthesized to increase pharmacological activity and reduce side effects [3].

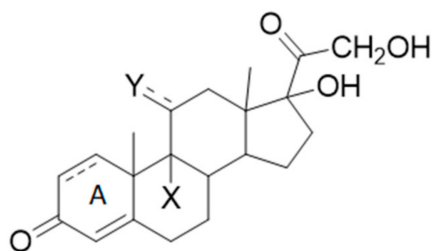
Due to their therapeutic properties and low cost, GCs are currently the most frequently used class of drugs to treat rheumatic and inflammatory diseases. As recently reported, the yearly number of prescribed GCs largely exceeds that of estrogens and androgens [4], although their use as doping agents and prophylactic in husbandry was banned by the World Anti-Doping Agency and by the Council Directive 96/22/EC, respectively [5,6].

Their occurrence in freshwaters, mainly as the initial drugs or slightly metabolized compounds, suggests that urban wastewater treatment plants (WWTPs) cannot remove

them quantitatively [7]. Indeed, just as many other drugs, they have been detected worldwide in the aquatic environment. River concentrations are in the ng L^{-1} or sub- ng L^{-1} range in European [4,8–11] and non-European countries [12–16]. On the other hand, significantly higher levels, ranging from few tens to some hundred nanograms per liter, have been measured in WWTPs and hospital wastewaters [17]. In particular, influent WWTPs contain massive GCs amounts, up to $2 \mu\text{g L}^{-1}$. Besides, some tens of ng per gram have been found in sewage sludge samples [9,18].

These concentrations are high enough to cause a negative eco-toxicological impact on various aquatic organisms, as demonstrated by the plethora of papers devoted to this issue. Under these conditions, reproduction, growth, and development of aquatic biota are affected by chronic exposure to low levels of GCs [19–22]. It was also reported that GCs act additively [22] and have cumulative effects in mixture with other steroid classes [20]. Depollution is a critical issue because of their negligible volatility and low biodegradability in urban WWTPs [7].

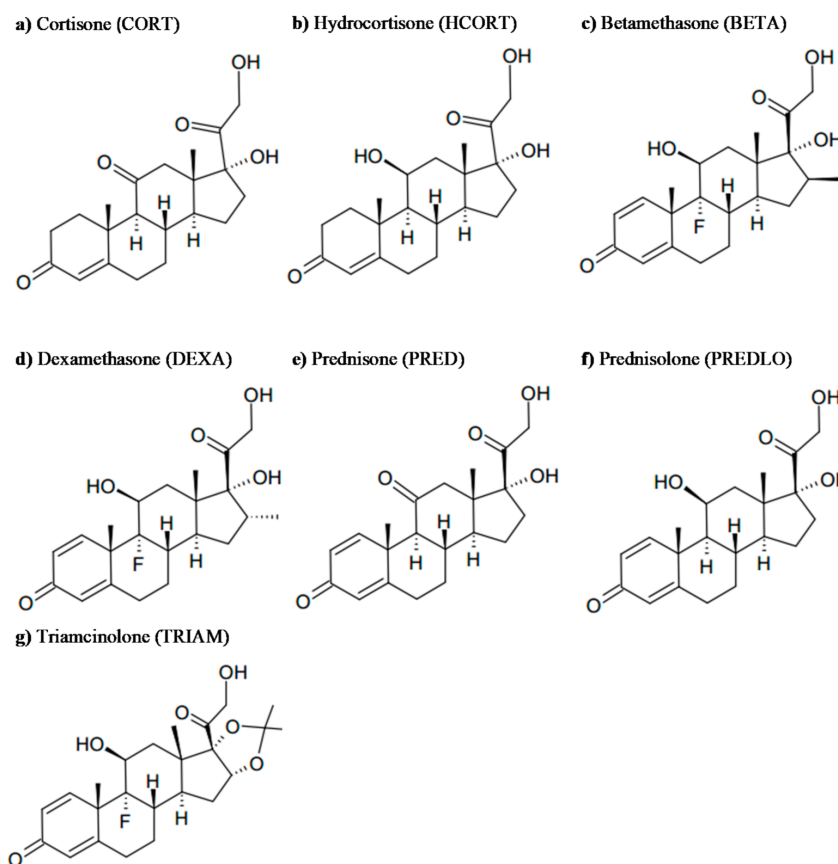
Due to the above, new strategies to abate GCs and those emerging contaminants of the aquatic environment that affect endogenous steroid actions have to be taken into account. In a recent paper [23], we studied the possibility of addressing this issue through direct photolysis in natural water. However, GCs photoreactivity under environmental conditions was found to be almost negligible due to their rigid cyclopentaperhydropenathrene structure and their limited light absorption in such highly diluted solutions, also when a more absorbing moiety, such as cross-conjugated chromophore in ring A, was present in the structure (see Scheme 1, X = H, F, Y = OH, O).



Scheme 1. The general structure of glucocorticoids (GCs).

We then decided to explore the possibility of improving the light-driven depollution process by adding a photocatalyst into the equation. Photocatalytic degradation of organic pollutants, such as drugs, has already demonstrated to be a highly effective process, also compared with other advanced oxidation processes (AOPs), and titania semiconductor oxides, under both UV-A and solar light ([24–26] and references therein). To date, the effectiveness of TiO_2 photocatalysis for removing GCs under actual conditions, viz. low-level concentrations and natural waters, has not yet been investigated. Only a few studies are available dealing with the TiO_2 -photocatalytic degradation of DEXA [27], CORT acetate [28], and PREDLO [29] under experimental conditions (mg per liter concentration, ultrapure water), quite different from the ones mentioned above.

In this work, a range of GCs was chosen among the largely prescribed natural and semisynthetic drugs (see Scheme 2) and were submitted to irradiation using a solar simulator and natural sunlight, in tap and river water at micrograms per liter concentration ($50 \mu\text{g L}^{-1}$).



Scheme 2. Structures of the GCs examined in this study.

The potential effect due to some of the main matrix constituents on GCs-TiO₂ photoreaction was also investigated.

Further experiments were carried out at mg per liter concentration (10 mg L⁻¹) to identify the primary photodegradation products by HPLC-ESI-MS/MS and elucidate the general photochemical path of GCs.

Finally, the sunlight TiO₂-photocatalytic efficiency for GCs removal was highlighted and compared with other advanced oxidation processes recently proposed [30–36].

2. Materials and Methods

2.1. Reagents and Materials

All the chemicals were of reagent grade or higher in quality and were used without any further purification. GCs standards (CORT, HCORT, BETA, DEXA, PRED, and PREDLO), acetic acid (99–100%), High-Performance Liquid Chromatography (HPLC) gradient-grade acetonitrile (ACN), CaSO₄ (99%), MgNO₃ hexahydrate (97%), and Humic acid sodium salt (MW = 100,000–150,000) were purchased by Merck (Milan, Italy). TRIAM was supplied by Farmabios (Gropello Cairoli, Italy). Methanol and water for Liquid Chromatography-Mass Spectrometry (LC/MS) were purchased by Carlo Erba Reagents (Cornaredo, Milano, Italy). GCs stock solutions of 10 mg L⁻¹ were prepared in tap water and stored in the dark at 4 °C for a maximum of a week. The working solution of 50 µg L⁻¹ was prepared daily. Aereoxide P25 titanium dioxide (Evonik, Resource Efficiency GmbH, Germany) was used for the photocatalytic experiments.

Nylon syringe filters (0.2 µm, 13 mm, Whatman, Milano, Italy) were used immediately after sample collection and before HPLC injection.

Tap water was from the Pavia municipal waterworks, while river water sample was collected from the Staffora River at 30–50 cm-depth in amber glass bottles. All the samples

were stored in the dark (4 °C) before use. The physico-chemical parameters are reported in Table 1.

Table 1. Physico-chemical characterization of tap and river water samples.

Parameters/Ions		Tap Water	River Water
pH		7.7	7.9
Conductivity at 20 °C	$\mu\text{S cm}^{-1}$	271	293
TOC *	mg L^{-1}	<2	6.9
Cl^{-}	mg L^{-1}	5.0	4.0
NO_3^{-}	mg L^{-1}	0.6	1.5
SO_4^{2-}	mg L^{-1}	5.0	13
HCO_3^{-}	mg L^{-1}	182	195
Ca^{2+}	mg L^{-1}	35	54
Mg^{2+}	mg L^{-1}	10	7.5
Na^{+}	mg L^{-1}	12	5.5

* TOC total organic carbon.

2.2. Analytical Determination

HPLC systems with different sensitivity and analysis modes were used. For the kinetic experiments at 10 mg L^{-1} , the HPLC-UV system consisted of a Shimadzu (Shimadzu Corporation, Milano, Italy) LC-20AT solvent delivery module equipped with a DGU-20A3 degasser and interfaced with a SPD-20A UV detector. The wavelength selected for analysis was 238 nm for all GCs. Each sample was diluted (30% *v/v*) with MeOH and injected (20 μL) into a $250 \times 4.6 \text{ mm}$, 5 μm GraceSmart RP18 (Sepachrom) coupled with a similar guard-column. The mobile phase was ultrapure water and ACN mixture, 70:30 for CORT, HCORT, PRED, and PREDLO; 65:35 for BETA, DEXA and TRIAM at a flow rate of 1.0 mL. The isocratic elution was maintained for 20 min, and then, after washing with 100% ACN for 5 min, the initial conditions were re-established. The instrumental quantification limits were 0.3 mg L^{-1} for CORT, HCORT, and DEXA, 0.09 mg L^{-1} for BETA, 0.2 mg L^{-1} for PRED, PREDLO, and TRIAM.

For the kinetic experiments at $50 \mu\text{g L}^{-1}$, the HPLC-ESI-MS/MS system consisted of an Agilent (Cernusco sul Naviglio, Milano, Italy) HPLC apparatus 1260 Infinity coupled with an Agilent 6460C ESI-MS/MS spectrometer. Each sample (5 μL) was injected into an Agilent 120 EC-C18 Poroshell column ($50 \times 3 \text{ mm}$, 2.7 μm) with a similar guard-column. The column temperature was maintained at $50 \pm 1 \text{ }^\circ\text{C}$. The mobile phases were (A) ultrapure water (0.1% *v/v* acetic acid) and (B) MeOH (0.1% *v/v* acetic acid). A linear gradient from 40% to 84% B was applied in 12 min, followed by a column re-equilibration time of 8 min. The flow rate was 0.6 mL min^{-1} .

GCs identification and quantification were performed in negative electrospray ionization (ESI). Source parameters were set as follows: drying gas temperature $300 \text{ }^\circ\text{C}$ (N_2); drying gas flow 5 L min^{-1} (N_2); nebulizer 45 psi; sheath gas temperature $250 \text{ }^\circ\text{C}$; sheath gas flow 11 L min^{-1} ; capillary voltage at 3500 V (positive mode) and 3000 V (negative mode); nozzle voltage 500 V positive, 0 V negative; electron multiplier voltage (EMV) 0 V for both polarities. MRM conditions (precursor ion $[\text{M} + \text{AcO}]^{-}$ adduct) for each compound are reported in Table S1. MassHunter Software from Agilent was used for data processing.

The HPLC-ESI-MS/MS analyses for photoproducts identification were performed by using a surveyor HPLC system (Thermo Finnigan, San Jose, CA, USA), equipped with a $150 \times 2.0 \text{ mm}$, 4 μm Jupiter 4U Proteo column (Phenomenex). The mobile phase consisted in: (A) ultrapure water (0.1% *v/v* formic acid) and (B) ACN (0.1% *v/v* formic acid). The starting concentration of eluent B was 2%, increased to 100% by 40 min with a linear gradient; this concentration was maintained for 5 min to wash the column. The flow rate was 0.2 mL min^{-1} . The MS/MS system consisted of an LCQ ADV MAX ion-trap mass spectrometer, with an ESI ion source operating in ion-positive mode with the following instrument conditions: source voltage 5.0 kV; capillary voltage 46 V; capillary

temperature 210 °C; tube lens voltage 55 V. Xcalibur 2.0.7 SP1 Software (Thermo Finnigan, San Jose, CA, USA) was used for spectra processing.

2.3. Irradiation Experiments

Irradiation experiments under simulated sunlight were carried out using a solar simulator (Solar Box 1500e, CO.FO.ME.GRA, Milano, Italy) set at a power factor 250 W m^{-2} (equipped with a UV outdoor filter of soda-lime glass IR-treated, and with a BST temperature sensor), and under natural sunlight. The incident power of natural sunlight (Pavia, $45^{\circ}11' \text{ N}$, $9^{\circ}09' \text{ E}$, June–July 2017, 12.00 a.m.–3.00 p.m., $27\text{--}30 \text{ }^{\circ}\text{C}$) was measured by means of an HD 9221 (Delta OHM, 450–950 nm) and a Multimeter (CO.FO.ME.GRA, 295–400 nm) pyranometers and resulted in the range $400\text{--}501 \text{ W m}^{-2}$ (Vis) and $22\text{--}34 \text{ W m}^{-2}$ (UV). The experiments were performed in a closed glass container containing 100 mL of untreated tap or river water samples (depth 40 mm, exposed surface 9500 mm^2) at native pH, enriched with $50 \mu\text{g L}^{-1}$ of each drug, separately dissolved and magnetically stirred. Aliquots (0.5 mL) of each sample were withdrawn at planned times, filtered, and injected in HPLC-ESI-MS/MS system (multiple reaction monitoring mode, MRM) to follow the degradation profiles.

Each kinetic experiment was performed in triplicate, and the degradation kinetic constant (k_{deg}) was calculated by using dedicated software (Fig P application, Fig P Software Corporation, version 2.2a, BIOSOFT, Cambridge, UK).

Before irradiation, each suspension ($50 \mu\text{g L}^{-1}$ of each GC, $0.5 \text{ g L}^{-1} \text{ TiO}_2$) was magnetically stirred in the dark for 20 min to promote the drug adsorption on the catalyst surface. For each GC, a control solution with no catalyst was also measured. No changes in GCs concentration were detected in the control samples.

To investigate matrix effects, a set of experiments, as described above, were carried out with the addition of salts (SO_4^{2-} 50 mg L^{-1} , NO_3^- 20 mg L^{-1}) and humic acids (HAs, 10 and 5 mg L^{-1}).

For identifying the photoproducts, 100 mL tap water samples were spiked with 10 mg L^{-1} of each GC (separately dissolved) and irradiated under simulated solar light as described above. Aliquots (0.5 mL), treated as above, were injected into the HPLC-UV system before performing the HPLC-ESI-MS/MS analysis (in full scan, zoom scan, and MS/MS mode).

3. Results and Discussion

We investigated TiO_2 photocatalytic degradation of seven most prescribed GCs (see Scheme 2) under relevant environmental conditions. To better mimic the realistic GCs degradation, a set of experiments were carried out on freshwater samples (not filtered tap and river water samples, native pH) enriched with $50 \mu\text{g L}^{-1}$ of each GC under simulated and natural sunlight. Photoproducts structures were determined by HPLC-ESI-MS/MS.

Results were discussed and compared to the most recently reported data obtained employing different advanced degradation techniques [30–36].

3.1. Kinetic Degradation in Actual Samples

The degradation profiles of the investigated GCs ($50 \mu\text{g L}^{-1}$) in tap (a) and river (b) water samples under simulated solar light are shown in Figure 1.

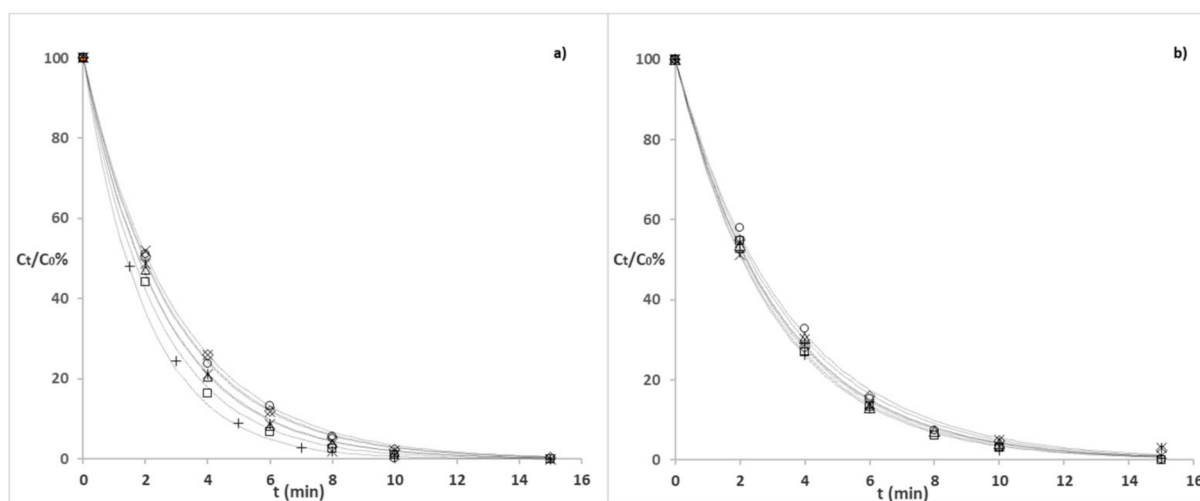


Figure 1. Evolution profiles of each GC ($50 \mu\text{g L}^{-1}$) in tap (a) and river water (b) under simulated sunlight: CORT (\diamond), HCORT ($*$), BETA (\times), DEXA (\triangle), PRED (\square), PREDLO ($+$), and TRIAM (\circ) (see Section 2.3 for the irradiation conditions).

A pseudo-first-order equation (see Equation (1)) satisfactorily fitted all of the experimental data:

$$\frac{C_t}{C_0} = e^{-k_{deg}t} \quad (1)$$

C_0 is the initial GC concentration, C_t is GC concentration at time t , and k_{deg} is the kinetic degradation constant.

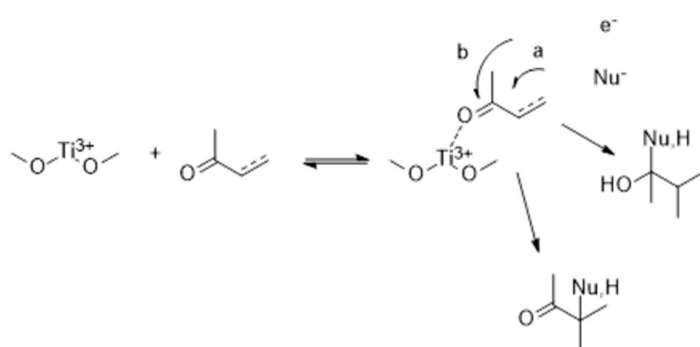
Table 2 shows the photolytic and photocatalytic degradation constants observed under the different experimental conditions described above.

Table 2. Observed GCs degradation constants (k_{deg}) ($50 \mu\text{g L}^{-1}$ GCs, 0.5 g L^{-1} TiO_2 , tap and river water, simulated, and natural sunlight).

Compound	Photolysis Simulated Solar Light		Photocatalysis Simulated Solar Light		Natural Sunlight
	Tap Water k_{deg} (min^{-1})	River Water k_{deg} (min^{-1})	Tap Water k_{deg} (min^{-1})	River Water k_{deg} (min^{-1})	River Water k_{deg} (min^{-1})
CORT	0.00106(5)	0.00128(3)	0.35(3)	0.300(8)	0.39(1)
HCORT	0.00246(9)	0.0033(2)	0.38(1)	0.315(8)	0.38(2)
BETA	0.0115(6)	0.0114(1)	0.336(9)	0.32(1)	0.35(2)
DEXA	0.0117(1)	0.0097(6)	0.386(9)	0.314(7)	0.61(1)
PRED	0.0185(9)	0.0186(6)	0.431(9)	0.33(1)	0.474(9)
PREDLO	0.024(1)	0.0199(4)	0.51(1)	0.336(4)	0.52(1)
TRIAM	0.0139(3)	0.0099(4)	0.355(9)	0.29(1)	0.38(1)

In brackets, the standard deviation values (sd), R^2 values in the range 0.992–0.999.

The most relevant result is that GCs direct photolysis occurred slowly, particularly for those GCs that scarcely absorb solar light (CORT and HCORT), with no significant difference between tap and river waters. On the contrary, TiO_2 -assisted photocatalysis appeared to be independent of the chemical structure of the GCs. It was much faster than the direct photolysis, one order of magnitude for the less persistent studied GCs (PRED and PREDLO) and up to two orders of magnitude for the more persistent ones (CORT and HCORT). Both observations are well in accord with the drug initial adsorption on the TiO_2 granule surface, which is known to happen mostly through the carbonyl function (see Scheme 3), with no considerable effect on the rest of the molecule.



Scheme 3. Initial adsorption of the drugs on the TiO₂ granule surface through the carbonyl function. As it is generally assumed, within TiO₂ crystals the titanium nuclei are bound to six oxygen anions in a bipyramid. However, the outermost titanium ions are not fully compensated by the oxygen charge and bear some positive charge. Complexation then involves a Ti³⁺ ion on the surface of the TiO₂ granule and the n orbital in the carbonyl function, as it happens in the acid catalysis of the addition to α , β -carbonyl onto the β (a) or carbonyl (b) functions [37,38].

As previously reported in the literature [29], GCs degradation is then expected to proceed mainly via the photocatalytic oxidation of the adsorbed molecules on the catalyst surface. This reaction is initiated on the surface of the catalyst, but the generated reactive intermediates are susceptible to a cascade of oxidative processes, which may happen both at the catalyst surface and in the nearby solution where photoproducted OH radicals also play a role. Likewise, the decrease in the decomposition rate, observed when a fluorine atom is introduced on the GC scaffold, well fits with the proposed mechanistic scheme (Scheme 3).

No significant difference in the order of reactivity was observed in the photocatalytic GCs degradation at mg per liter concentration; a quantitative GCs removal ($\geq 95\%$) under actual conditions (natural pH, untreated water sample, and simulated sunlight) occurred in 15 min for all GCs. The observed kinetic degradation constants (k_{deg}) calculated for each GC are shown in Table 3.

Table 3. Degradation constants (k_{deg}) for each GC (10 mg L⁻¹) in tap water under simulated sunlight (see Paragraph 2.3 for the irradiation conditions) and comparison with other AOPs.

GC	AOP	Matrix	Kinetic Constant, % Removal, Degradation Time	Ref
DEXA 2-50 mg L ⁻¹	Gamma ray, gamma ray with H ₂ O ₂ or Fenton	Pure water, pH 7.2	$5 \times 10^{-4} - 4.7 \times 10^{-3} \text{ Gy}^{-1}$, $8 \times 10^{-4} - 1.6 \times 10^{-3} \text{ Gy}^{-1}$	[35]
PRED 50 mg L ⁻¹	Electrochemical oxidation process 20 mA cm ⁻²	Pure water, pH 11, Na ₂ SO ₄ 1 g L ⁻¹	0.1052 mg h ⁻¹ , 78% removal 4 h	[33]
PRED acetate 5 mg L ⁻¹	O ₃ 50 mg min ⁻¹	Pure water, pH 3	0.0595 min ⁻¹ , 90% removal 30 min	[32]
PREDLO 3.6 mg L ⁻¹	UV/chlorine, 254 nm	Phosphate buffer pH 7, artificial fresh water pH 6	$5.53 \times 10^{-3} \text{ s}^{-1}$	[31]
PREDLO 100 mg L ⁻¹	UV-Fenton, 360 nm	Pure water, pH 3	Quantitative removal 15 min	[30]
DEXA 5 mg L ⁻¹	ZrO ₂ 1.5 g L ⁻¹ , 365 nm WO ₃ 0.5 g L ⁻¹ , >380 nm	Pure water, pH 3	ZrO ₂ 0.0078 min ⁻¹ , 76% removal 180 min WO ₃ 0.0277 min ⁻¹ , 100% removal 80 min	[34]

Table 3. Cont.

GC	AOP	Matrix	Kinetic Constant, % Removal, Degradation Time	Ref
BETA phosphate 30 mg L ⁻¹	ZnO 0.44 g L ⁻¹ , 254 nm ZnO 0.44 g L ⁻¹ , persulfate, 254 nm	Pure water, pH 9	Removal 63%, 180 min Removal 98%, 180 min	[36]
PREDLO 25 mg L ⁻¹	TiO ₂ P25 1 g L ⁻¹ , 365 nm or solar light	Pure water, pH 6.7	Removal 94%, 1 h solar light Removal 73%, 1 h 365 nm	[29]
CORT acetate 10 mg L ⁻¹	TiO ₂ P25, 375 nm, air saturated, TiO ₂ P25, 375 nm, persulfate air saturated	Different buffer solution, air saturated	0.040 min ⁻¹ , quantitative removal 100 min, 0.071 min ⁻¹ , quantitative removal 30 min	[28]
DEXA 10 mg L ⁻¹	TiO ₂ P25 0.2 g L ⁻¹ , simulated solar light	Pure water, air saturated	Quantitative removal 15 min	[27]
CORT, HCORT, BETA, DEXA, PRED, PREDLO, TRIAM 10 mg L ⁻¹	TiO ₂ P25 0.5 g L ⁻¹ , simulated solar light	Tap water, natural pH	0.184(5), 0.230(7), 0.19(1), 0.206(5), 0.177(7), 0.224(3), 0.24(1) min ⁻¹ Removal >95% 15 min	[This work]

These results are particularly informative for evaluating the validity of TiO₂ remediation in real matrices under UV-A or solar light compared with other advanced oxidation processes, such as ZnO [36] WO₃ and ZrO₂ [34] semiconductors, ozone [32], gamma irradiation [35], UV/chlorine process [31], photo-Fenton [30] and electrochemical oxidation process [33]. For example, ZnO has a low stability in aqueous solutions at natural pH [36]; WO₃ and ZrO₂ require strong acidic conditions to work [34]. Other AOPs, such radiolysis [35] or photo-Fenton [30], need the addition of a sacrificial oxidizing agent (H₂O₂, S₂O₈²⁻, etc.) to improve their photocatalytic performance; ozonization [32] and electrochemical oxidation process [33] require acidic and alkaline solutions, respectively, and UV/chlorine process [31] occurs under UV-C irradiation.

None of the above-mentioned AOPs is competitive in terms of GCs degradation rate if compared to TiO₂, and, importantly, they have never been applied to GCs degradation at µg L⁻¹ levels in environmental conditions.

3.2. Matrix Effects: Salts and Humic Acids

As opposed to photolysis, GCs TiO₂-mediated photodegradation took place slightly slower in river samples than in tap water samples. It was faster under natural sunlight in river water than simulated light (see Table 2), proving the process efficiency despite changeable environmental factors, such as incident power [39]. Despite the similar qualitative composition of the two considered matrices (see Table 1), a decrease in k_{deg} was observed for all GCs in river water samples than in tap water samples under the same experimental conditions (see Table 2). We attempted to evaluate the potential matrix contribution to this effect, although, in general, this is a challenging task, especially in real matrices where the many species present may interact with each other and also with several other xenobiotics [40].

Among the various macro-constituents, nitrate and sulfate were investigated because they are more abundant than others in the considered river water sample (see Table 1) and, at the same time, are known to affect drug photodegradation [40], including GCs. Indeed, some previous works reported the influence of SO₄²⁻ and NO₃⁻ on the AOPs degradation rate of GCs. In particular, SO₄²⁻ was found to reduce the photodegradation rate of BETA [36], PREDLO [31], and PRED [32], acting directly as hydroxyl radical scavenger to form the respective anion radicals; NO₃⁻ was reported to slow down the decomposition rate of DEXA decreasing OH radical concentration indirectly via NO₂⁻ [35]. Other important interferents naturally present in river water are humic acids (HAs); these ubiquitous

species can act both as photo-sensitizers or compete in absorbing solar light [40,41]. Recent studies examined the inhibition effect of natural organic matter (NOM) on the degradation rate of PREDLO [31] and showed that increasing the NOM concentration, k_{deg} decreased.

Based on the k_{deg} values reported in Table 2 and on the GCs structures, three model GCs, viz. CORT, PREDLO, and TRIAM were selected, and their photodegradation was investigated in tap water fortified with the above-mentioned inorganic salts and HAs, following the procedure described in Section 2.3. Salt concentrations (some tens of mg per liter) higher than those measured in the river water samples were specifically added to evidence their potential impact on the GCs degradation rate, while HAs levels, corresponding to 7.5 mg L^{-1} of total organic carbon (TOC), were added to mimic the natural organic matter present in the river sample (see Table 1). Irradiation was carried out in tap water by a solar light simulator. The degradation rates were calculated and reported in Table 4.

Table 4. Photodegradation constants (k_{deg}) determined in tap water under simulated sunlight in the presence of inorganic salts and humic acids (HAs).

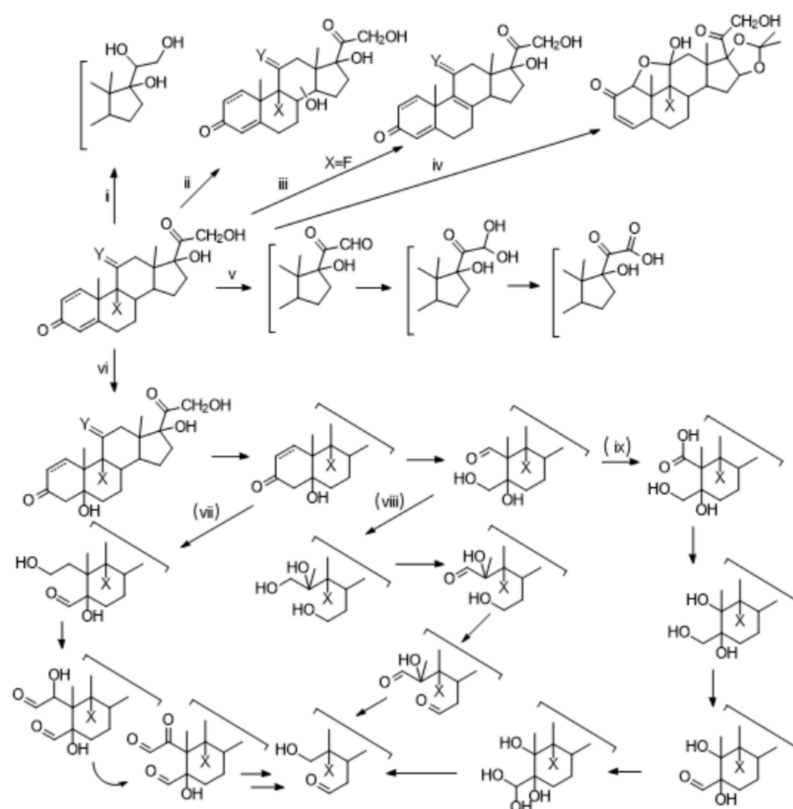
Compound	CORT	PREDLO	TRIAM
Matrix	$k_{deg} \text{ (min}^{-1}\text{)}$		
tw	0.35 (3)	0.51 (1)	0.355 (9)
tw + SO_4^{2-} (50 mg L^{-1})	0.41 (3)	0.539 (5)	0.31 (1)
tw + NO_3^- (20 mg L^{-1})	0.28 (1)	0.45 (1)	0.37 (1)
tw + HAs (10 mg L^{-1})	0.10 (1)	0.10 (1)	0.08 (1)

As showed in Table 4, the added SO_4^{2-} (50 mg L^{-1}) had a small or no effect on the degradation rates of the chosen GCs, while NO_3^- (20 mg L^{-1}) slightly affected the degradation rates, in the order CORT > PREDLO > TRIAM. On the contrary, HAs (10 mg L^{-1}) had the most significant impact on all drugs, from 4- to 5-fold decrease of the rate. Interestingly, no significant differences in k_{deg} were observed in a more diluted HAs solution (5 mg L^{-1}) for the considered GCs. As expected, competitive light absorption by dissolved organic matter deviated significantly the process from the photocatalytic path.

3.3. Identification of Photoproducts

As mentioned above, all the studied GCs underwent a fast decomposition both in tap and river water.

HPLC-ESI-MS/MS qualitative analysis revealed many photoproducts (see Supplementary Materials), and some trends can be identified based on the structure of the starting GCs. Six main reaction pathways can be described, involving either the hydroxyacetyl side chain or the steroid ring (see Scheme 4) and two of them, viz. (iv), cyclohexadienone isomerization, only available for those GCs containing a second conjugated double bond, and (v), the photooxidation of C17 side chain, have been already described as the main reaction paths in the direct photolysis of glucocorticoids ([23] and references therein). Nonetheless, the products coming from these two routes are now a minority among the identified degradation mechanisms, and we were able to characterize byproducts from path (iv) only for TRIAM (see Supplementary Materials), while the importance of path (v) is highly reduced with respect to direct photolysis, especially for those GCs having a second conjugated double bond on ring A.



Scheme 4. Paths followed in the photocatalytic degradation of GCs.

Among the remaining four main pathways, route (i) is a minority process only observed for CORT, HCORT, and PRED, and it comes from the formal reduction of the carbonyl at C17. The same is true for path (iii), which led to the reductive dehalogenation of DEXA. The latter reaction has been previously described for DEXA-phosphate photochemistry in the presence of a reducing agent [42]. Both path (i) and (ii) can be related to the free electrons generated on the catalyst surface upon irradiation reacting with adsorbed GCs at the catalyst surface. Nevertheless, most of the identified photoproducts are peculiar of the photocatalytic process, not produced under direct photolysis [23], and can be directly linked to OH radicals photo-generated from the irradiated TiO₂ catalyst. This powerful oxidant can then attack the steroid backbone either on C4=C5 double bond on ring A, path (vi), leading to double bond hydration followed by ring-opening, as already reported in the literature for PREDLO [29], then starting a cascade reaction (path vii, viii, and ix), ultimately yielding highly degraded products, or via OH insertion on the internal rings, (ii) producing hydroxylated byproducts [27]. The preference toward one or more of these degradation paths for the seven studied GCs can be rationalized by looking at their molecular structure, where the not-conjugated CORT and HCORT prefer to undergo path (ii) or (v), so reacting either at the C17 hydroxyacetyl side chain or via OH insertion on the inner steroid rings, while the GCs bearing a second double bond on ring A shift the preferred OH attack to this site (path vi), resulting in a C5–OH pivotal intermediate which then further reacts (path vii, viii, and ix) forming several different oxidized byproducts. Nonetheless, path (ii) and (v) do not completely disappear but contribute to the overall photodegradation process to a lesser extent. In accordance with the proposed mechanism, we saw that the addition of NO₃[−] (20 mg L^{−1}) to tap water impacts the degradation rates in the order CORT > PREDLO > TRIAM; this can be tentatively rationalized based on NO₃[−] scavenging effects on both OH radicals and photogenerated e_{aq}[−], involving mostly the single conjugated CORT chemistry where the lack of the second double bond impairs competitive degradation paths, viz. double bond hydration (vi) and cyclohexadienone isomerization (iv). On the contrary, the effect of HAs is independent of the chemical structure of the studied GCs and can

be explained with HAs competing both with TiO_2 for light absorption and with GCs for the adsorption sites on the catalyst surface. As previously mentioned, other secondary processes are still available for those GCs having particular structures, viz. reductive defluorination for DEXA, cyclohexadienone isomerization for TRIAM.

4. Conclusions

The present study proves that TiO_2 -assisted photocatalysis effectively removes various GCs present in freshwaters at μg per liter levels. Degradations occurred within 15 min for all GCs, and they were found to be from one to two orders of magnitude higher than direct photolysis, also in the case of CORT and HCORT that scarcely absorb solar light. The photoproducts formed during the first steps of the photocatalytic process, with a lifetime comparable to that of their parent compounds, were identified and allowed to elucidate the general mechanistic path. As indicated above, two main paths, different from those observed in the direct photolysis experiments, dominate the GCs photooxidation, involving either the unsaturated ketone moiety in ring A, especially for those GCs having a second conjugated double bond, or the C-H bonds on the steroid ring, with a limited number of isomers, which ultimately demonstrate that the process initiates from the TiO_2 -drug complex.

In contrast to what was seen from photolytic experiments, we found that GCs photodegradation in the presence of TiO_2 proceeds slightly faster in tap water than in river water due to natural interferents such as HAs and inorganic anions more abundant in the latter. Nonetheless, TiO_2 photodegradation remained effective and faster than direct photolysis, also in the presence of matrix constituents, such as natural organic matter and salts, ubiquitous species in freshwaters. Furthermore, the reaction was shown to be efficient under natural solar light thanks to the photocatalyst ability to absorb in a wide range of wavelengths. The degradation mechanism is dominated by OH radicals generated on the catalyst surface, which then react with adsorbed GCs following different paths based on the particular chemical structure of each drug, while products from direct photolysis are still present but as a minority. Furthermore, even if the kinetic reaction constants are comparable across all the studied GCs, from an environmental point of view, it is important to underline that those compounds bearing a second conjugated double bond on ring A have access to a wider range of degradation paths, leading in the end to the formation of more degraded byproducts which mostly lost the pharmacologically active steroid ring.

Once again, photocatalysis was shown to be the method of choice for water depollution. The mechanism may change somewhat, but the great stability of the titania crystals under irradiation, coupled with the good adsorption properties and catalytic activity, overcome any other method.

Supplementary Materials: The following are available online at <https://www.mdpi.com/2076-3417/11/6/2486/s1>, Table S1: Optimized MRM conditions for the HPLC-ESI-MS/MS analysis, Table S2: Fragmentation of photolytic products of CORT ($[\text{M} + 1]^+ = 361$), Table S3: Fragmentation of photolytic products of HCORT ($[\text{M} + 1]^+ = 363$), Table S4: Fragmentation of photolytic products of BETA ($[\text{M} + 1]^+ = 393$). Table S5: Fragmentation of photolytic products of DEXA ($[\text{M} + 1]^+ = 393$), Table S6: Fragmentation of photolytic products of PRED ($[\text{M} + 1]^+ = 359$), Table S7: Fragmentation of photolytic products of PREDLO ($[\text{M} + 1]^+ = 361$), Table S8: Fragmentation of photolytic products of TRIAM ($[\text{M} + 1]^+ = 435$).

Author Contributions: Conceptualization, M.S., A.A., L.P. and F.M.; formal analysis, M.S.; investigation, A.C. and S.N.; writing—original draft preparation, M.S., L.P. and A.A.; writing—review and editing, M.S., L.P., F.M. and S.N.; visualization, M.S., L.P., A.C. and F.M. All authors have read and agreed to the published version of the manuscript.

Funding: This research received no external funding.

Institutional Review Board Statement: Not applicable.

Informed Consent Statement: Not applicable.

Data Availability Statement: The data presented in this study are available on request from the corresponding author.

Conflicts of Interest: The authors declare no conflict of interest.

References

1. Ramamoorthy, S.; Cidlowski, J.A. Corticosteroids. *Rheum. Dis. Clin. N. Am.* **2016**, *42*, 15–31. [CrossRef] [PubMed]
2. Oakley, R.H.; Cidlowski, J.A. The biology of the glucocorticoid receptor: New signaling mechanisms in health and disease. *J. Allergy Clin. Immunol.* **2013**, *132*, 1033–1044. [CrossRef] [PubMed]
3. Bolster, M.B. Corticosteroids: Friends and Foes. *Rheum. Dis. Clin. N. Am.* **2016**, *42*, xv–xvi. [CrossRef] [PubMed]
4. Jia, A.; Wu, S.; Daniels, K.D.; Snyder, S.A. Balancing the Budget: Accounting for Glucocorticoid Bioactivity and Fate during Water Treatment. *Environ. Sci. Technol.* **2016**, *50*, 2870–2880. [CrossRef]
5. Duclos, M. Glucocorticoids: A Doping Agent? *Endocrinol. Metab. Clin. N. Am.* **2010**, *39*, 107–126. [CrossRef]
6. EEC council directive No. 96/22/EC. *Off. J. Eur. Commun. L* **1996**, *125*. Available online: <https://eur-lex.europa.eu/legal-content/EN/ALL/?uri=CELEX%3A31996L0023> (accessed on 14 February 2021).
7. Weizel, A.; Schlüsener, M.P.; Dierkes, G.; Wick, A.; Ternes, T.A. Analysis of the aerobic biodegradation of glucocorticoids: Elucidation of the kinetics and transformation reactions. *Water Res.* **2020**, *174*, 115561. [CrossRef] [PubMed]
8. Kugathas, S.; Williams, R.J.; Sumpter, J.P. Prediction of environmental concentrations of glucocorticoids: The River Thames, UK, as an example. *Environ. Int.* **2012**, *40*, 15–23. [CrossRef]
9. Herrero, P.; Borrull, F.; Pocurull, E.; Marcé, R.M. Determination of glucocorticoids in sewage and river waters by ultra-high performance liquid chromatography–tandem mass spectrometry. *J. Chromatogr. A* **2012**, *1224*, 19–26. [CrossRef]
10. Weizel, A.; Schlüsener, M.P.; Dierkes, G.; Ternes, T.A. Occurrence of Glucocorticoids, Mineralocorticoids, and Progestogens in Various Treated Wastewater, Rivers, and Streams. *Environ. Sci. Technol.* **2018**, *52*, 5296–5307. [CrossRef]
11. Speltini, A.; Merlo, F.; Maraschi, F.; Sturini, M.; Contini, M.; Calisi, N.; Profumo, A. Thermally condensed humic acids onto silica as SPE for effective enrichment of glucocorticoids from environmental waters followed by HPLC-HESI-MS/MS. *J. Chromatogr. A* **2018**, *1540*, 38–46. [CrossRef]
12. Wu, S.; Jia, A.; Daniels, K.D.; Park, M.; Snyder, S.A. Trace analysis of corticosteroids (CSs) in environmental waters by liquid chromatography–tandem mass spectrometry. *Talanta* **2019**, *195*, 830–840. [CrossRef]
13. Fan, Z.; Wu, S.; Chang, H.; Hu, J. Behaviors of Glucocorticoids, Androgens and Progestogens in a Municipal Sewage Treatment Plant: Comparison to Estrogens. *Environ. Sci. Technol.* **2011**, *45*, 2725–2733. [CrossRef] [PubMed]
14. Chang, H.; Hu, J.; Shao, B. Occurrence of Natural and Synthetic Glucocorticoids in Sewage Treatment Plants and Receiving River Waters. *Environ. Sci. Technol.* **2007**, *41*, 3462–3468. [CrossRef] [PubMed]
15. Shen, X.; Chang, H.; Sun, Y.; Wan, Y. Determination and occurrence of natural and synthetic glucocorticoids in surface waters. *Environ. Int.* **2020**, *134*, 105278. [CrossRef]
16. Gong, J.; Lin, C.; Xiong, X.; Chen, D.; Chen, Y.; Zhou, Y.; Wu, C.; Du, Y. Occurrence, distribution, and potential risks of environmental corticosteroids in surface waters from the Pearl River Delta, South China. *Environ. Pollut.* **2019**, *251*, 102–109. [CrossRef] [PubMed]
17. Schriks, M.; van Leerdam, J.A.; van der Linden, S.C.; van der Burg, B.; van Wezel, A.P.; de Voogt, P. High-Resolution Mass Spectrometric Identification and Quantification of Glucocorticoid Compounds in Various Wastewaters in The Netherlands. *Environ. Sci. Technol.* **2010**, *44*, 4766–4774. [CrossRef] [PubMed]
18. Guedes-Alonso, R.; Santana-Viera, S.; Montesdeoca-Esponda, S.; Afonso-Olivares, C.; Sosa-Ferrera, Z.; Santana-Rodríguez, J.J. Application of microwave-assisted extraction and ultra-high performance liquid chromatography–tandem mass spectrometry for the analysis of sex hormones and corticosteroids in sewage sludge samples. *Anal. Bioanal. Chem.* **2016**, *408*, 6833–6844. [CrossRef]
19. Willi, R.A.; Faltermann, S.; Hettich, T.; Fent, K. Active Glucocorticoids Have a Range of Important Adverse Developmental and Physiological Effects on Developing Zebrafish Embryos. *Environ. Sci. Technol.* **2018**, *52*, 877–885. [CrossRef] [PubMed]
20. Willi, R.A.; Castiglioni, S.; Salgueiro-González, N.; Furia, N.; Mastroianni, S.; Faltermann, S.; Fent, K. Physiological and Transcriptional Effects of Mixtures of Environmental Estrogens, Androgens, Progestins, and Glucocorticoids in Zebrafish. *Environ. Sci. Technol.* **2020**, *54*, 1092–1101. [CrossRef] [PubMed]
21. Xin, N.; Jiang, Y.; Liu, S.; Zhou, Y.; Cheng, Y. Effects of prednisolone on behavior and hypothalamic–pituitary–interrenal axis activity in zebrafish. *Environ. Toxicol. Pharmacol.* **2020**, *75*, 103325. [CrossRef]
22. Willi, R.A.; Salgueiro-González, N.; Carcaiso, G.; Fent, K. Glucocorticoid mixtures of fluticasone propionate, triamcinolone acetonide and clobetasol propionate induce additive effects in zebrafish embryos. *J. Hazard. Mater.* **2019**, *374*, 101–109. [CrossRef] [PubMed]
23. Cantalupi, A.; Maraschi, F.; Pretali, L.; Albin, A.; Nicolis, S.; Ferri, E.N.; Profumo, A.; Speltini, A.; Sturini, M. Glucocorticoids in freshwaters: Degradation by solar light and environmental toxicity of the photoproducts. *Int. J. Environ. Res. Public Health* **2020**, *17*, 8717. [CrossRef] [PubMed]
24. Gmurek, M.; Olak-Kucharczyk, M.; Ledakowicz, S. Photochemical decomposition of endocrine disrupting compounds – A review. *Chem. Eng. J.* **2017**, *310*, 437–456. [CrossRef]

25. Serpone, N.; Artemev, Y.M.; Ryabchuk, V.K.; Emeline, A.V.; Horikoshi, S. Light-driven advanced oxidation processes in the disposal of emerging pharmaceutical contaminants in aqueous media: A brief review. *Curr. Opin. Green Sustain. Chem.* **2017**, *6*, 18–33. [[CrossRef](#)]
26. Pretali, L.; Maraschi, F.; Cantalupi, A.; Albin, A.; Sturini, M. Water Depollution and Photo-Detoxification by Means of TiO₂: Fluoroquinolone Antibiotics as a Case Study. *Catalysts* **2020**, *10*, 628. [[CrossRef](#)]
27. Calza, P.; Pelizzetti, E.; Brussino, M.; Baiocchi, C. Ion trap tandem mass spectrometry study of dexamethasone transformation products on light activated TiO₂ surface. *J. Am. Soc. Mass Spectrom.* **2001**, *12*, 1286–1295. [[CrossRef](#)]
28. Romão, J.S.; Hamdy, M.S.; Mul, G.; Baltrusaitis, J. Photocatalytic decomposition of cortisone acetate in aqueous solution. *J. Hazard. Mater.* **2015**, *282*, 208–215. [[CrossRef](#)] [[PubMed](#)]
29. Klauson, D.; Pilnik-Sudareva, J.; Pronina, N.; Budarnaja, O.; Krichevskaya, M.; Käkinen, A.; Juganson, K.; Preis, S. Aqueous photocatalytic oxidation of prednisolone. *Open Chem.* **2013**, *11*, 1620–1633. [[CrossRef](#)]
30. Díez, A.M.; Ribeiro, A.S.; Sanromán, M.A.; Pazos, M. Optimization of photo-Fenton process for the treatment of prednisolone. *Environ. Sci. Pollut. Res.* **2018**, *25*, 27768–27782. [[CrossRef](#)] [[PubMed](#)]
31. Yin, K.; He, Q.; Liu, C.; Deng, Y.; Wei, Y.; Chen, S.; Liu, T.; Luo, S. Prednisolone degradation by UV/chlorine process: Influence factors, transformation products and mechanism. *Chemosphere* **2018**, *212*, 56–66. [[CrossRef](#)]
32. He, X.; Huang, H.; Tang, Y.; Guo, L. Kinetics and mechanistic study on degradation of prednisone acetate by ozone. *J. Environ. Sci. Health Part A* **2020**, *55*, 292–304. [[CrossRef](#)] [[PubMed](#)]
33. Welter, J.B.; da Silva, S.W.; Schneider, D.E.; Rodrigues, M.A.S.; Ferreira, J.Z. Performance of Nb/BDD material for the electrochemical advanced oxidation of prednisone in different water matrix. *Chemosphere* **2020**, *248*, 126062. [[CrossRef](#)] [[PubMed](#)]
34. Ghenaatgar, A.; Tehrani, R.M.A.; Khadir, A. Photocatalytic degradation and mineralization of dexamethasone using WO₃ and ZrO₂ nanoparticles: Optimization of operational parameters and kinetic studies. *J. Water Process Eng.* **2019**, *32*, 100969. [[CrossRef](#)]
35. Guo, Z.; Guo, A.; Guo, Q.; Rui, M.; Zhao, Y.; Zhang, H.; Zhu, S. Decomposition of dexamethasone by gamma irradiation: Kinetics, degradation mechanisms and impact on algae growth. *Chem. Eng. J.* **2017**, *307*, 722–728. [[CrossRef](#)]
36. Giah, M.; Taghavi, H.; Habibi, S. Photocatalytic degradation of betamethasone sodium phosphate in aqueous solution using ZnO nanopowder. *Russ. J. Phys. Chem. A* **2012**, *86*, 2003–2007. [[CrossRef](#)]
37. Thomas, A.G.; Syres, K.L. Adsorption of organic molecules on rutile TiO₂ and anatase TiO₂ single crystal surfaces. *Chem. Soc. Rev.* **2012**, *41*, 4207. [[CrossRef](#)] [[PubMed](#)]
38. Sushko, M.L.; Gal, A.Y.; Shluger, A.L. Interaction of organic molecules with the TiO₂ (110) surface: Ab initio calculations and classical force fields. *J. Phys. Chem. B* **2006**, *110*, 4853–4862. [[CrossRef](#)] [[PubMed](#)]
39. Sturini, M.; Speltini, A.; Maraschi, F.; Profumo, A.; Pretali, L.; Fasani, E.; Albin, A. Photochemical Degradation of Marbofloxacin and Enrofloxacin in Natural Waters. *Environ. Sci. Technol.* **2010**, *44*, 4564–4569. [[CrossRef](#)] [[PubMed](#)]
40. Petala, A.; Mantzavinos, D.; Frontistis, Z. Impact of water matrix on the photocatalytic removal of pharmaceuticals by visible light active materials. *Curr. Opin. Green Sustain. Chem.* **2021**, *28*, 100445. [[CrossRef](#)]
41. Vione, D. Photochemical reactions in sunlit surface waters: Influence of water parameters, and implications for the phototransformation of xenobiotic compounds. *Photochemistry* **2016**, *44*, 348–363.
42. Rasolevandi, T.; Naseri, S.; Azarpira, H.; Mahvi, A.H. Photo-degradation of dexamethasone phosphate using UV/Iodide process: Kinetics, intermediates, and transformation pathways. *J. Mol. Liq.* **2019**, *295*, 111703. [[CrossRef](#)]